Analyst

RSC Publishing

PAPER

Breast cancer and melanoma cell line identification by FTIR imaging after formalin-fixation and paraffin-embedding

Cite this: *Analyst*, 2013, **138**, 4083

M. Verdonck,†[a] N. Wald,†[a] J. Janssis,[a] P. Yan,[b] C. Meyer,[c] A. Legat,[c] D. E. Speiser,[c] C. Desmedt,[d] D. Larsimont,[e] C. Sotiriou[d] and E. Goormaghtigh*[a]

Over the past few decades, Fourier transform infrared (FTIR) spectroscopy coupled to microscopy has been recognized as an emerging and potentially powerful tool in cancer research and diagnosis. For this purpose, histological analyses performed by pathologists are mostly carried out on biopsied tissue that undergoes the formalin-fixation and paraffin-embedding (FFPE) procedure. This processing method ensures an optimal and permanent preservation of the samples, making FFPE-archived tissue an extremely valuable source for retrospective studies. Nevertheless, as highlighted by previous studies, this fixation procedure significantly changes the principal constituents of cells, resulting in important effects on their infrared (IR) spectrum. Despite the chemical and spectral influence of FFPE processing, some studies demonstrate that FTIR imaging allows precise identification of the different cell types present in biopsied tissue, indicating that the FFPE process preserves spectral differences between distinct cell types. In this study, we investigated whether this is also the case for closely related cell lines. We analyzed spectra from 8 cancerous epithelial cell lines: 4 breast cancer cell lines and 4 melanoma cell lines. For each cell line, we harvested cells at subconfluence and divided them into two sets. We first tested the "original" capability of FTIR imaging to identify these closely related cell lines on cells just dried on BaF_2 slides. We then repeated the test after submitting the cells to the FFPE procedure. Our results show that the IR spectra of FFPE processed cancerous cell lines undergo small but significant changes due to the treatment. The spectral modifications were interpreted as a potential decrease in the phospholipid content and protein denaturation, in line with the scientific literature on the topic. Nevertheless, unsupervised analyses showed that spectral proximities and distances between closely related cell lines were mostly, but not entirely, conserved after FFPE processing. Finally, PLS-DA statistical analyses highlighted that closely related cell lines are still successfully identified and efficiently distinguished by FTIR spectroscopy after FFPE treatment. This last result paves the way towards identification and characterization of cellular subtypes on FFPE tissue sections by FTIR imaging, indicating that this analysis technique could become a potential useful tool in cancer research.

Received 31st January 2013
Accepted 30th April 2013

DOI: 10.1039/c3an00246b

www.rsc.org/analyst

Introduction

Over the past few decades, Fourier transform infrared (FTIR) spectroscopy coupled to microscopy has been recognized as an emerging tool for histopathological studies.[1–3] This technique provides spatially resolved information on the chemical composition of the sample based on the vibrational signature of the tissue components.[4] Because of its potential to probe chemical constituents without dyes or specific reagents, FTIR imaging could become a powerful tool in diagnosis to complement the existing methods.[2] In cancer research, FTIR imaging has proven its worth in the study of a large panel of different cancers: cervix,[5] breast,[6] prostate,[7] lung,[8,9] colon,[10] skin,[11] liver,[12] oesophagus[13] or brain cancer.[14]

Histological analyses performed by pathologists are mostly carried out on biopsies that undergo a fixation process followed by staining.[2] The standard tissue processing method is the formalin-fixation and paraffin-embedding (FFPE) procedure.[15] The FFPE procedure allows durable and optimal preservation of

[a]*Laboratory for the Structure and Function of Biological Membranes, Center for Structural Biology and Bioinformatics, Université Libre de Bruxelles, Campus Plaine, Bld du Triomphe 2, CP206/2, B1050 Brussels, Belgium. E-mail: egoor@ulb.ac.be; Fax: +32-2-650-53-82; Tel: +32-2-650-53-86*

[b]*Institute of Pathology CHUV, University of Lausanne, Switzerland*

[c]*Ludwig Center for Cancer Research, Department of Oncology CHUV, University of Lausanne, Lausanne, Switzerland*

[d]*Breast Cancer Translational Research Laboratory, Institut Jules Bordet, Brussels, Belgium*

[e]*Pathological Anatomy Department, Institut Jules Bordet, Brussels, Belgium*

† These authors contributed equally to this work.

the structure of the biopsied tissue required for histopathological analyses. By blocking autolysis and by crosslinking the primary and secondary amine groups of proteins, this fixation process allows long-term conservation.[16] More precisely, the FFPE process involves a first step of fixation by formalin, followed by a second step of dehydration with increasing ethanol concentrations and finally addition of xylene to create a hydrophobic environment before paraffin embedding. Paraffin plays the role of a support needed to cut tissue sections of a few micrometers which can then be deposited on a microscope slide.[17] These FFPE-archived tissues, which are easy to handle and economical to store, are an extremely valuable source of samples for retrospective studies. For these practical reasons, most histological studies performed worldwide are made on FFPE tissues.[18]

Nevertheless, it is well documented that the formalin-based fixation has significant effects on the biochemical composition of cells and tissues.[19] FFPE potentially impacts all the major constituents of the cells (proteins, lipids, RNA, DNA…).[18,20,21] This fact raises some questions both for biologists and spectroscopists.[20,22] Previous studies have been carried out in order to describe the influence of formalin-based fixation and paraffin preservation on spectral features of tissues and cells with both infrared and Raman spectroscopy.[16,19,23–30] While some studies report only a slight impact of formalin fixation on the spectra,[26,28–30] other studies observed important modifications concerning the cellular lipid and protein content.[19,23,25,27] Pleshko *et al.* also demonstrated in 1992 an effect of ethanol on amide I and II of proteins.[24] Despite these chemical modifications, this technique allows precise identification of the different cell types present in biopsied tissues,[2,31] indicating that the FFPE process preserves spectral differences between distinct cell types.

In this study, we attempt to determine whether the FFPE process preserves spectral differences between very similar cell lines. To address this question, we analyzed spectra acquired from 8 cancerous epithelial cell lines: 4 breast cancer cell lines and 4 melanoma cell lines. We first tested the "original" capability of FTIR imaging to identify these closely related cell lines, on cells just dried on BaF_2 slides. We repeated the test after submitting the cells to the FFPE procedure. We finally discuss the discriminatory power and FFPE-induced spectral modifications.

Materials and methods

1 Cell culture

The 4 human breast carcinoma cell lines (MCF7, MDAMB231, SKBR3, and T47D) were acquired from the American Type Culture Collection (ATCC, Manassas, VA). Melanoma cell lines (Me260, Me275, T50B, and T1353A) were acquired from metastases from patients with cutaneous melanoma at the Ludwig Center of Cancer Research in Lausanne, Switzerland. They were extracted from fresh surgery samples using mechanical and enzymatic dissociation. The Me275 and T50B cell lines come from two separate surgeries of the same patient with 12 years of interval.[32] All the cell lines were grown at 37 °C in a constant humidified atmosphere of 5% CO_2 in air. The cell lines were cultured to 80% confluence in RPMI 1640 medium supplemented with 10% FBS, 1% L-glutamine and 1% penicillin/streptomycin. Only for the melanoma cell lines 1% non-essential amino acid was added to the medium. Cell culture medium, FBS and antibiotics were purchased from Lonza (Verviers, Belgium). Cell cultures were tested for mycoplasma infection every other week using PlasmoTest (InvivoGen, France). Each culture was executed twice, at distinct times, in order to duplicate the complete experiment.

2 FFPE procedure and dried fixation

Once the cells reached subconfluence *i.e. ca.* 80% confluence, they were detached from their culture support by means of a 5 minute treatment with trypsin (0.5 g l^{-1})/EDTA (0.2 g l^{-1}) buffer (Lonza, Verviers, Belgium). Culture medium was added to stop the action of trypsin and the cells were pelleted by a 2 minute centrifugation (231 × *g*). The cells were then washed three times with an isotonic solution of NaCl (0.9%) to completely remove trypsin and culture medium. After this step, a part (1/8) of the cells was deposited on a BaF_2 slide and air-dried before infrared measurements. For the other parts of the cells, the FFPE treatment was followed. After a 4 hour incubation at room temperature in 4% formalin solution (QPath, Labonord SAS, France), cells were packed in paper provided for that purpose before being immersed in a series of baths as described in Table 1. The cell pellet was then embedded in paraffin and 3 μm thick sections were cut and mounted on BaF_2 slides. Paraffin was removed with a 10 minute incubation of the sample in xylene.

3 FTIR measurements

The IR data were collected using a Hyperion 3000 IR imaging system (Bruker Optics, Ettlingen, Germany), equipped with a liquid nitrogen cooled 64 × 64 Mercury Cadmium Telluride (MCT) Focal Plane Array (FPA) detector. The data were collected in transmission mode. The size of an image covers an area of 180 × 180 μm^2 composed of 4096 pixels of 2.8 × 2.8 μm^2. It must be noted that spatial resolution is significantly lower than the pixel size, depending on the wavelength, *i.e.* 5 μm at 2000 cm^{-1} and 10 μm at 1000 cm^{-1}. It took about 5 minutes to record 256 scans at a spectral resolution of 8 cm^{-1}. Ten images were recorded for each sample. Spectra were therefore acquired on several hundreds of cells for each cell line in each condition (dried or FFPE).

Table 1 FFPE procedure of the cell lines: solvents, times and incubation temperatures

Chemical	Concentration (%)	Incubation time (h)	Incubation temperature (°C)
Buffered formalin (pH 7)	10	2	37
Ethanol	70	1	37
Ethanol	97	2	37
Isopropanol	100	3	37
Xylene	100	3	37
Paraffin	100	2.5	59

4 Data analysis

4.1 Preprocessing. All spectra were preprocessed as follows. Water vapor contribution was subtracted as described previously[33,34] with 1956–1935 cm^{-1} as the reference peak and the CO_2 peak was flattened between 2450 and 2250 cm^{-1}. The spectra were baseline-corrected. Straight lines were interpolated between the spectral points at 3620, 2995, 2800, 2395, 2247, 1765, 1724, 1480, 1355, 1144 and 950 cm^{-1} and subtracted from each spectrum. Spectra were normalized for equal area between 1725 and 1481 cm^{-1} (amide I and II peaks). The signal to noise ratio (*S*/*N*) was then systematically checked on every spectrum. It was required to be greater than 300 when noise was defined as the standard deviation in the 2000–1900 cm^{-1} region of the spectrum and the signal was the maximum of the curve between 1750 and 1480 cm^{-1} after subtracting a baseline through these two points. Finally, some rare spectra with normalized absorbance lower than −5 (negative lobe) and a maximum above 120 (saturation) were discarded. To avoid abrupt refractive index changes we always selected areas of the sample with contiguous cells. Visual inspection of spectra as well as systematic screening for negative lobes on the left hand side of the ester carbonyl did not reveal significant dispersive artifacts. There is an ongoing debate about dispersive artifact correction, with different methods and softwares being used, *e.g.* ref. 35–37. As these corrections rely on simplified models and as dispersive artifacts were minor in the present work, we preferred not to apply such a correction.

4.2 Difference spectra. Difference spectra allow emphasizing the spectral variations between two distinct conditions. Difference spectra were built by a subtraction of the mean spectrum of the dried cells from the mean spectrum of the FFPE preserved cells.

4.3 Statistical analyses. In order to observe the intrinsic proximities and distances within the dataset and to group spectra according to their similarity, some unsupervised analyses were achieved. Hierarchical cluster analyses (HCA) using Ward's algorithm, as already described,[38,39] and principal component analyses (PCA) were performed. Supervised analysis was also conducted on the dataset. Partial least squares discriminant analysis was done to extract latent variables of the dataset that enable the construction of a factor capable of predicting a class.

Correction of the spectra for water vapor contribution, baseline subtraction and normalization, hierarchical classification, principal component analysis and partial least squares discriminant analysis were carried out by Kinetics, a custom made program, running under Matlab (Matlab, Mathworks Inc).

Results

Epithelial cancerous cell lines, including 4 breast cancer (MCF7, MDAMB231, SKBR3, T47D) and 4 melanoma cell lines (T1353, T50B, Me275, Me260) were grown to subconfluence, resuspended in 0.9% NaCl, pelleted by centrifugation and either simply dried on BaF_2 windows or formalin-fixed, paraffin-embedded, cut in 3 μm thick slices and de-waxed, as described in the Materials and methods. For each of the 8 cancerous cell lines considered, 20 infrared images were recorded for both the dried and the FFPE conditions. A field of view of an infrared image was covered by approximately 40 cells. In a first step, after preprocessing, the FTIR spectra obtained from each IR image were averaged to obtain one mean spectrum, as illustrated in Fig. 1. Examination of those spectra indicates that, for one given cell line, the mean IR spectra are quite similar for both conditions. Yet, the FFPE treatment induced some minor but noticeable changes.

1 Does the FFPE treatment induce similar spectral changes for different cell lines?

In order to highlight the spectral modifications brought by the FFPE procedure, difference spectra were computed. Difference

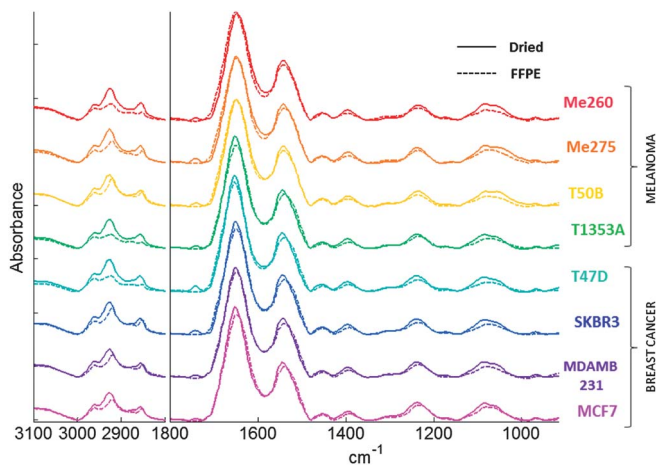

Fig. 1 Mean IR spectra of the 4 melanoma and 4 breast cancer cell lines, indicated in the right margin, in the dried (solid lines) and FFPE (dotted-lines) conditions. Each spectrum is the average of *ca.* 10 000 spectra. Spectra are offset for visual clarity.

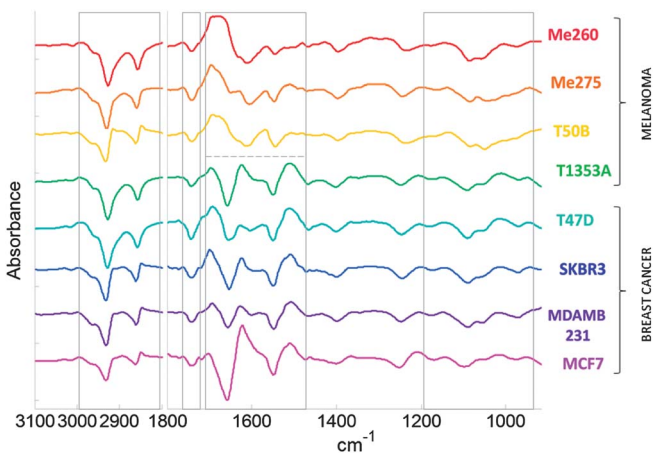

Fig. 2 Difference spectra of the 8 epithelial cancerous cell lines. The spectra were obtained by subtracting, for each cell line, the mean IR spectra of the dried cells from the mean IR spectra of the FFPE processed cells. The various cell lines are indicated in the right margin. Spectra are offset for visual clarity.

spectra, illustrated in Fig. 2, were obtained by subtracting, for each cell line, the mean spectra of the dried cells from their FFPE counterparts.

As shown in Fig. 2, the difference spectra present a high degree of similarity over the whole spectral region, irrespective of the cell line. This suggests that, in this study, the FFPE treatment influences the IR spectra of the various breast cancer and melanoma cell lines in a similar way.

A closer look at the difference spectra indicates that most differences could be hypothetically assigned to the loss of phospholipids. In particular, we observe a group of negative peaks in the 3000–2800 cm^{-1} region that can be assigned to methyl (2960 cm^{-1}) and methylene (2925, 2850 cm^{-1}) stretching vibrations associated with lipid acyl chains, a negative band around 1750–1735 cm^{-1} corresponding to the carbonyl stretching absorption of lipid esters as well as several negative peaks in the phosphate absorption region (1200–900 cm^{-1}).[40,41]

Fig. 2 underlines another spectral characteristic shared by the majority of the difference spectra, consisting of a negative peak around 1655 cm^{-1} and a positive peak near 1630 cm^{-1}. This particular pattern could reasonably be assigned to a change in the protein secondary structure upon FFPE treatment. Indeed, this spectral feature could be explained as a shift in the maximum of the amide I peak from near 1655 cm^{-1} to 1630 cm^{-1}, reminiscent of a transition from α-helix structures into β-sheet structures.[42,43] Interestingly, this conformational change is not observed for all cell lines, in particular for 3 melanoma cell lines. This was found to be related to the melanin content and will be discussed later.

To test the hypothesis that FFPE processing results in the loss of phospholipids and protein conformational change, a "synthetic" difference spectrum, illustrated in Fig. 3, was built by linear combination of the IR spectrum of a protein rich in α-helices (hemoglobin), the spectrum of a protein rich in β-sheets (concanavalin A) and the spectrum of a phospholipid, dioleoylphosphatidylcholine (DOPC). The weight of each of the three components was computed to best fit the SKBR3 difference spectrum in the least squares sense (Fig. 3). The synthetic difference spectrum generally shows a high degree of similarity with the cell line difference spectrum.

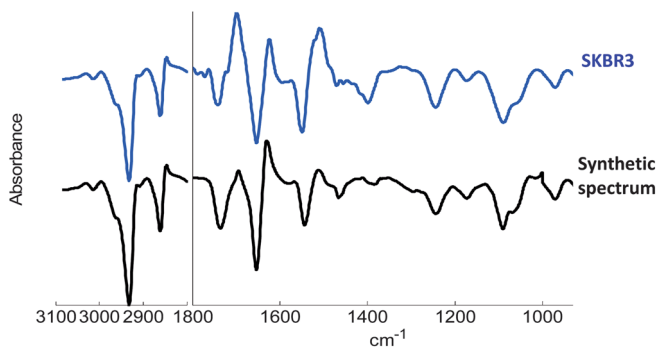

Fig. 3 Difference spectrum of the SKBR3 breast cancer cell line (FFPE – dried) (above) and synthetic spectrum (below) constructed by linear combination of the IR spectrum of a protein rich in α-helices (hemoglobin), the spectrum of a protein rich in β-sheets (concanavalin A) and the spectrum of a phospholipid (DOPC). The weight of each of the three components was computed to obtain the best fit of the SKBR3 difference spectrum in the least squares sense. Spectra are offset for visual clarity.

2 Are spectral proximities and distances between closely related cell lines conserved after FFPE processing?

While it is known that the FFPE process preserves spectral differences between highly distinct cell types (*i.e.* lymphocytes, epithelial cells, erythrocytes and fibroblasts) on biological tissue sections,[31] it has not been clearly established yet whether the FFPE procedure maintains spectral differences and distances that could exist between closely related cellular subtypes. Hierarchical Cluster Analysis (HCA) and Principal Component Analysis (PCA) group spectra according to their similarity and allow the intrinsic proximities and distances within the dataset to be observed.

Fig. 4 illustrates hierarchical cluster analyses obtained for the mean IR spectra of the breast cancer (Fig. 4A) and melanoma cell lines (Fig. 4B). Both analyses were performed on the two combined 3000–2800 and 1800–900 cm^{-1} spectral regions, which include the IR absorption bands of main biological molecules. As can be seen in Fig. 4A, the principal segregation is related to the treatment (dried or FFPE). Examination of the dendrogram under both conditions reveals that cell line spectra that cluster in the dried condition (*i.e.* SKBR3, MDAMB231, and MCF7) also cluster after FFPE treatment and the cell line spectrum that was the most distant in the dried condition (*i.e.* T47D) was also the most distant in the FFPE condition. HCA of the melanoma cell lines (Fig. 4B) also shows clustering according to the treatment. Even though the dendrogram patterns within the two conditions (dried and FFPE) are significantly different, the spectra of the two cell lines that originate from the same patient (*i.e.* T50B and Me275) cluster in both conditions. This unsupervised statistical analysis thus indicates that the spectral proximities and distances between dried cell lines are not totally conserved after the FFPE procedure. Nonetheless, general trends are maintained.

Fig. 5A reports a PCA score plot for the first two principal components (*i.e.* PC1 *versus* PC2). As revealed by the cluster analysis (Fig. 4), the cell lines mainly cluster according to the condition (dried or FFPE). Interestingly, when scores on the PC3 and PC4 principal components of the PCA are examined (Fig. 5B), the spectra rather group as a function of the cell line, irrespective of the treatment. This indicates that PC1 and PC2 extract common spectral changes related to FFPE processing while PC3 and PC4, illustrated in Fig. 5B, reflect variability related to the nature of the cell line. The latter observation indicates that spectral features specific to each cell line are likely to be conserved even after the major alteration by the FFPE treatment.

In Fig. 4 and 5, the PCA and HCA are performed on the mean IR spectra of each cell line.

Those analyses therefore do not bring any information about the statistical significance of the classification obtained. There is in fact a significant degree of overlap when presenting individual spectra on the HCA or PCA plot. This reflects the fact

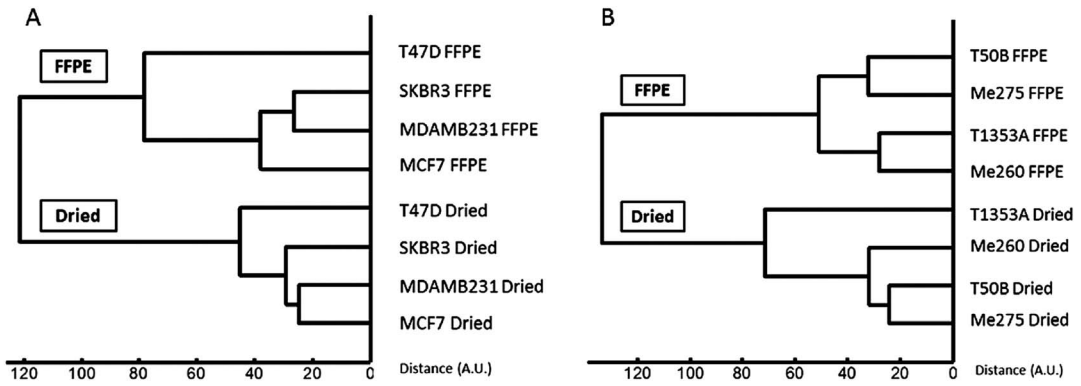

Fig. 4 Hierarchical cluster analyses of the mean IR spectra presented in Fig. 1, of the two combined 3000–2800 and 1800–900 cm^{-1} spectral regions. (A) Hierarchical cluster analysis of the mean IR spectra of the breast cancer cell lines, (B) hierarchical cluster analysis of the mean IR spectra of the melanoma cell lines.

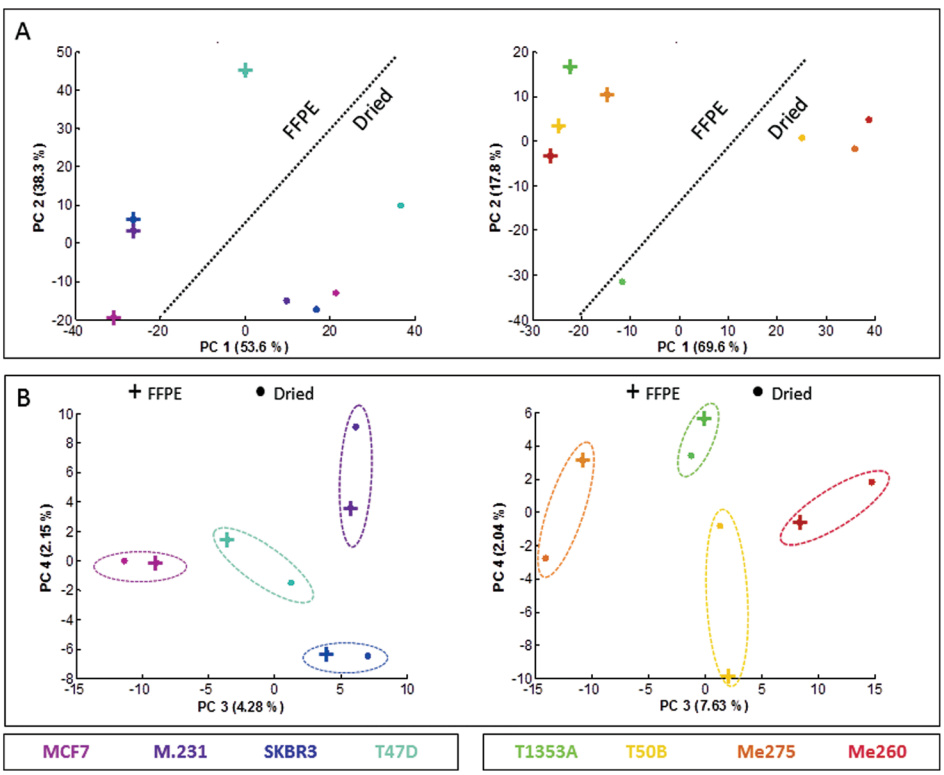

Fig. 5 Principal component analyses of the mean IR spectra presented in Fig. 1, of the 1800–900 cm^{-1} spectral region. (A) PCA score plots for the first two principal components (*i.e.* PC1 *versus* PC2), for the breast cancer (left) and melanoma cell lines (right). (B) PCA score plots for the principal components PC3 and PC4, for the breast cancer (left) and melanoma cell lines (right).

that, when considering the entire dataset, unsupervised analyses do not perfectly separate the different cell lines and conditions (approximately 300 000 individual spectra are obtained). Furthermore, the huge amount of data would result in highly overlapping clouds of dots in the case of principal component analyses and dendrograms with a colossal number of branches getting muddled up, in the case of hierarchical cluster analyses. On the other hand, when statistical analyses were performed on the mean spectra of each cell line in each condition, taking into account the individual spectra, highly significant differences between the means were found (not shown). A MANOVA analysis indicated that the differences between the means are always very significant with alpha values <0.01% for any pair of means. For this reason, to visualize the relative distance between the means, we present HCA and PCA on these means.

3 Is supervised discrimination power between cell lines conserved after FFPE processing?

Principal Least Squares Discriminant Analysis (PLS-DA), a supervised statistical analysis, was applied to all individual

Table 2 Validation of the cell line recognition models: confusion matrices obtained for the PLS-DA supervised statistical analyses on the two combined 3000–2800 and 1800–900 cm^{-1} spectral regions. For each cell line, in both conditions (dried or FFPE), a first batch of spectra including two thirds of the IR spectra was used to train the model (training set); the remaining third was included in a second batch of spectra and used to test the model (test set). The percentages found in the confusion matrices represent the capability of the model to predict the second batch of spectra. At least 7600 IR spectra were considered per cell line and condition. One confusion matrix (*i.e.* validation of PLS-DA models) was obtained using approximately 40 000 IR spectra. Percentages in the matrices indicate the rate of correct assignment of the spectra to the cell line. The error on the percentage corresponds to the standard deviation obtained after 40 bootstrapping iterations. (A) Confusion matrices obtained when applying the cell line recognition models for the breast cancer (left) and melanoma (right) cell lines in the dried condition. (B) Confusion matrices obtained when applying the cell line recognition models for the breast cancer (left) and melanoma (right) cell lines in the FFPE condition

A

Dried cell lines		Predicted as: MCF7	MDAMB 231	SKBR3	T47D
True	MCF7	98.5 ± 0.2	0.6 ± 0.1	0.9 ± 0.1	0.1 ± 0.0
	MDAMB 231	0.3 ± 0.1	97.6 ± 0.3	0.0 ± 0.0	2.0 ± 0.3
	SKBR3	1.6 ± 0.3	0.0 ± 0.0	98.1 ± 0.3	0.3 ± 0.1
	T47D	0.2 ± 0.1	0.1 ± 0.0	0.9 ± 0.2	98.7 ± 0.2

Dried cell lines		Predicted as: T1353A	T50B	Me275	Me260
True	T1353A	97.1 ± 0.2	0.8 ± 0.2	0.2 ± 0.1	1.9 ± 0.2
	T50B	0.3 ± 0.1	99.3 ± 0.1	0.2 ± 0.1	0.2 ± 0.1
	Me275	0.4 ± 0.1	0.1 ± 0.1	99.5 ± 0.1	0.0 ± 0.0
	Me260	0.1 ± 0.0	0.2 ± 0.1	0.0 ± 0.0	99.6 ± 0.1

B

FFPE cell lines		Predicted as: MCF7	MDAMB 231	SKBR3	T47D
True	MCF7	98.3 ± 0.3	1.5 ± 0.2	0.2 ± 0.1	0.0 ± 0.0
	MDAMB 231	0.2 ± 0.1	99.4 ± 0.1	0.2 ± 0.1	0.3 ± 0.1
	SKBR3	0.1 ± 0.1	0.7 ± 0.1	99.0 ± 0.2	0.1 ± 0.1
	T47D	0.0 ± 0.0	0.0 ± 0.0	0.3 ± 0.1	99.7 ± 0.1

FFPE cell lines		Predicted as: T1353A	T50B	Me275	Me260
True	T1353A	98.0 ± 0.2	0.4 ± 0.1	1.6 ± 0.2	0.1 ± 0.0
	T50B	3.2 ± 0.3	95.8 ± 0.4	1.0 ± 0.2	0.0 ± 0.0
	Me275	0.2 ± 0.1	0.1 ± 0.0	99.7 ± 0.1	0.0 ± 0.0
	Me260	0.1 ± 0.0	0.1 ± 0.0	6.5 ± 0.4	93.3 ± 0.4

spectra obtained from IR images to account for the spectral diversity existing within one cell line. For every cell line in each condition (dried or FFPE), two thirds of the IR spectra recorded were used to train the classification model and the remaining third was used to test the model. The confusion matrices resulting from this validation are shown in Table 2. In these tables, the percentages indicate the rate of correct assignments of the spectra to the group (*i.e.* cell line) and the error on the percentage corresponds to the standard deviation computed after 40 bootstrapping iterations of the model.

As can be seen from Table 2A, the percentages of correct assignments of the IR spectra to each cell line are particularly high in the dried condition. Indeed, for both breast cancer and melanoma cell lines, percentages range between 97.1 and 99.6%, which indicates a very efficient identification. Similarly, Table 2B illustrates the confusion matrices obtained for the IR spectra of FFPE cells. The percentages of correct assignments obtained in this condition are also very high, ranging from 93.3 to 99.7%, revealing efficient recognition after the FFPE treatment of cells.

Discussion

In cancer research, most biological tissues stored for histological studies are formalin-fixed and paraffin-embedded. As detailed in the Introduction, FFPE specimens present numerous advantages, making the archived tissues an extremely valuable source of samples for retrospective studies.[15,18,20] Nevertheless, this fixation method has shown to impact the biochemical content and thus the infrared spectra of cells.[16,18,19,21–23,25,26,43] Previous studies indicate that different cell types present on a FFPE tissue section are still successfully identified by their IR spectra.[31,44] It remained to be demonstrated that FTIR imaging can distinguish the minor differences that exist between cellular subtypes. Here, very similar cell lines were examined before and after FFPE processing.

The cell lines used in this study were chosen because of their particular similarities. They are all well characterized cancerous epithelial cell lines. As indicated by the American Type Culture Collection (ATCC) from where they were purchased, the 4 breast cancer cell lines present similar DNA profiles. The melanoma cell lines all originate from melanoma metastases, and were extensively characterized.[32,45] Furthermore, 2 of the 4 melanoma cell lines were obtained from two biopsies carried out on the same patient.

In order to mimic the effects of FFPE processing used for tissues, the incubation times of the cell lines in the different solvents and paraffin were those usually applied to tissues, *i.e.* much longer than strictly required for the fixation of cells alone. This implies that the spectral modifications observed in Fig. 1 and 2 might be even more important than the changes occurring in the IR spectra of cells embedded inside a tissue.

Fig. 1 indicates that the spectrum of a cell line in the dried condition is only slightly different from its FFPE counterpart,

implying limited spectral changes due to the FFPE treatment. These results are in line with numerous previous studies which report only slight modifications of the spectra after formalin fixation[16,19,23,26,29,30] but contradict few others which attribute large spectral changes to fixation protocols.[25,27] Various studies indicate that other fixation methods used for the preservation of biological tissues influence similarly or even more the cell IR spectra. For instance, fixatives like acetone or ethanol are shown to influence more considerably the IR spectra of cells than formalin-fixation.[15,18,23,25] Interestingly, any other sample fixation method, including fresh-frozen tissues, usually considered as a reference of native state, or air drying, has an impact on the IR spectra of cells.[23,46]

As indicated in Fig. 2 and 3, the FFPE procedure induces similar modifications in the IR spectra of all cell lines. These spectral modifications could potentially be explained in terms of protein denaturation and a decrease in the phospholipid content. Yet, the particular shape of the difference spectra illustrated in Fig. 2 and 3 could also hypothetically correspond to a modification of the phosphate groups from the nucleic acids (the FFPE procedure is known to induce modifications on the RNA and DNA),[18,21,47] combined with a loss of triglycerides. However, a closer examination of the difference spectra of Fig. 2 and 3 highlights arguments for a loss of phospholipids. For instance, the band at 1172 cm^{-1} is observed in the IR spectrum of DOPC but not in the RNA or DNA spectrum (not shown). Furthermore, the 1090/1060 cm^{-1} ratio is superior to 1 for the difference spectra as well as for the spectra of DOPC, whereas it is inferior to 1 for RNA or DNA spectrum (not shown). The cause of protein conformational change remains undetermined. Numerous studies have shown that formalin affects only moderately the IR spectra of biological samples.[19,26,48] Consequently, any other solvent used in the FFPE process, alone or combined with another, is potentially responsible for the effects highlighted in the IR cell spectra. For instance, ethanol has been shown to impact the shape of amide I and II and xylene affects numerous peaks of the IR spectra of cells.[23,24] Finally, the heating step (*ca.* 59 °C) experienced during paraffin embedding could play a role in the protein denaturation observed on FFPE treated cells.

As shown in Fig. 2, the IR spectra of three melanoma cell lines containing melanin (*i.e.* T50B, Me275 and Me260) were differently affected by the FFPE process when compared to the amelanotic melanoma cell line T1353A or the breast cancer cell lines. It can be hypothesized that the presence of large amounts of melanin pigment is responsible for the difference. In general, the FFPE-induced spectral modification in the amide I region can be associated with a change in the protein secondary structure, from helical to sheet structures upon FFPE processing. This change was not observed for melanin-containing T50B, Me275 and Me260 cell lines. It could simply be masked by another modification of melanin overlapping the former one. Alternatively, the large positive band present around 1677 cm^{-1} in these difference spectra could be associated with the presence of newly formed beta-turns and random coil structures.[42,49]

In Fig. 4 and 5, we decided to analyze the two datasets (breast cancer and melanoma cell lines) separately for greater clarity. All cell lines (breast cancer and melanoma) used in this study are human epithelial cancer cell lines. These cell lines are intrinsically very similar and, when considered together for statistical analyses, data from both datasets tend to overlap, particularly when applying unsupervised statistical analyses.

The results presented in Table 2, indicating a correct identification of the cell types despite spectral modifications due to the fixation process, are in accordance with the literature. This report together with previous studies shows that spectral changes observed following formalin fixation are smaller than those due to biochemical changes associated with disease-induced effects or different cell types.[29,30,50]

In conclusion, FFPE processing is responsible for limited but significant modifications of the IR spectrum of cells. Nonetheless, distinctions between IR spectra of cellular subtypes are as accurate as before FFPE processing. These results suggest that FTIR imaging of FFPE tissue sections could become an efficient tool to distinguish very similar cells and classify cancer cells according to minute variations.

Abbreviations

DOPC	Dioleoylphosphatidylcholine;
FPA	Focal Plane Array;
FFPE	Formalin-Fixation Paraffin-Embedding;
FTIR	Fourier transform infrared;
HCA	Hierarchical Cluster Analysis;
IR	Infrared;
MCT	Mercury Cadmium Telluride;
PCA	Principal Component Analysis;
PC	Principal Component;
PLS-DA	Partial Least Squares Discriminant Analysis;
S/*N*	Signal to Noise.

Acknowledgements

The authors would like to give special acknowledgment to Ghizlane Rouas, from the Breast Cancer Translational Research Laboratory J.C. Heuson (BCTL) of Jules Bordet Institute, for her help and advice. Sincere thanks are also due to Donata Rimoldi and Katja Muehlethaler, from the Ludwig Center for Cancer Research of the University of Lausanne, for producing the melanoma cell lines used in this study. This research has been supported by grants from the National Fund for Scientific Research (FRFC 2.4533.10 and 2.4527.10, 2.4526.12 and T.0155.13), a grant from the Swiss Cancer League (KFS-2836-08-2011), and the Ludwig Institute for Cancer Research. E.G. is Director of Research with the National Fund for Scientific Research (FNRS) (Belgium), M.V. and N.W. are Research Fellows supported by the Fund for Research and Education within Industry and Agriculture (FRIA) from the FNRS (Belgium).

References

1 G. Bellisola and C. Sorio, *Am. J. Cancer Res.*, 2012, **2**, 1–21.
2 R. Bhargava, *Anal. Bioanal. Chem.*, 2007, **389**, 1155–1169.

3 P. Lasch, M. Diem, W. Hänsch and D. Naumann, *J. Chemom.*, 2007, **20**, 209–220.
4 P. Lasch, L. Chiriboga, H. Yee and M. Diem, *Technol. Cancer Res. Treat.*, 2002, **1**, 1–7.
5 M. J. Walsh, M. J. German, M. Singh, H. M. Pollock, A. Hammiche, M. Kyrgiou, H. F. Stringfellow, E. Paraskevaidis, P. L. Martin-Hirsch and F. L. Martin, *Cancer Lett.*, 2007, **246**, 1–11.
6 S. Rehman, Z. Movasaghi, A. T. Tucker, S. P. Joel, J. A. Darr, A. V. Ruban and I. U. Rehman, *J. Raman Spectrosc.*, 2007, **38**, 1345–1351.
7 J. T. Kwak, S. M. Hewitt, S. Sinha and R. Bhargava, *BMC Cancer*, 2011, **11**, 62.
8 P. D. Lewis, K. E. Lewis, R. Ghosal, S. Bayliss, A. J. Lloyd, J. Wills, R. Godfrey, P. Kloer and L. A. J. Mur, *BMC Cancer*, 2010, **10**, 640.
9 B. Bird, M. S. Miljković, S. Remiszewski, A. Akalin, M. Kon and M. Diem, *Lab. Invest.*, 2012, **92**, 1358–1373.
10 A. Travo, O. Piot, R. Wolthuis, C. Gobinet, M. Manfait, J. Bara, M.-E. Forgue-Lafitte and P. Jeannesson, *Histopathology*, 2010, **56**, 921–931.
11 P. T. Wong, S. M. Goldstein, R. C. Grekin, T. A. Godwin, C. Pivik and B. Rigas, *Cancer Res.*, 1993, **53**, 762–765.
12 F. Le Naour, M.-P. Bralet, D. Debois, C. Sandt, C. Guettier, P. Dumas, A. Brunelle and O. Laprévote, *PLoS One*, 2009, **4**, 1–10.
13 L. Quaroni and A. G. Casson, *Analyst*, 2009, **134**, 1240–1246.
14 C. Krafft, S. B. Sobottka, K. D. Geiger, G. Schackert and R. Salzer, *Anal. Bioanal. Chem.*, 2007, **387**, 1669–1677.
15 M. A. Perlmutter, C. J. M. Best, J. W. Gillespie, Y. Gathright, S. González, A. Velasco, W. M. Linehan, M. R. Emmert-Buck and R. F. Chuaqui, *J. Mol. Diagn.*, 2004, **6**, 371–377.
16 E. Gazi, J. Dwyer, N. P. Lockyer, J. Miyan, P. Gardner, C. Hart, M. Brown and N. W. Clarke, *Biopolymers*, 2005, **77**, 18–30.
17 J. Rieppo, L. Rieppo, S. Saarakkala and J. S. Jurvelin, in *Fourier Transforms – New Analytical Approaches and FTIR Strategies*, ed. G. S. Nikolic, InTech, 2011, pp. 3–14.
18 C. J. Huijsmans, J. Damen, J. C. van der Linden, P. H. Savelkoul and M. H. Hermans, *BMC Res. Notes*, 2010, **3**, 239.
19 A. D. Meade, C. Clarke, F. Draux, G. D. Sockalingum, M. Manfait, F. M. Lyng and H. J. Byrne, *Anal. Bioanal. Chem.*, 2010, **396**, 1781–1791.
20 M. Braun, R. Menon, P. Nikolov, R. Kirsten, K. Petersen, D. Schilling, C. Schott, S. Gündisch, F. Fend, K.-F. Becker and S. Perner, *BMC Cancer*, 2011, **11**, 511.
21 D. L. Evers, C. B. Fowler, B. R. Cunningham, J. T. Mason and T. J. O'Leary, *J. Mol. Diagn.*, 2011, **13**, 282–288.
22 D. Otali, C. R. Stockard, D. K. Oelschlager, W. Wan, U. Manne, S. A. Watts and W. E. Grizzle, *J. Lip. Res.*, 2010, **84**, 223–247.
23 E. O'Faolaoin, M. Hunter, J. Byrne, P. Kellehan, M. McNamara and F. Lying, *Dublin Inst. Technol.*, 2005, **38**, 121–127.
24 N. L. Pleshko, a. L. Boskey and R. Mendelsohn, *Calcif. Tissue Int.*, 1992, **51**, 72–77.
25 Z. Huang, A. McWilliams, S. Lam, J. English, D. I. McLean, H. Lui and H. Zeng, *Int. J. Oncol.*, 2003, **23**, 649–655.
26 G. Hastings, R. Wang, P. Krug, D. Katz and J. Hilliard, *Biopolymers*, 2008, **89**, 921–930.
27 M. M. Mariani, P. Lampen, J. Popp, B. R. Wood and V. Deckert, *Analyst*, 2009, **134**, 1154–1161.
28 A. C. Bot, A. Huizinga, F. F. de Mul, G. F. Vrensen and J. Greve, *Exp. Eye Res.*, 1989, **49**, 161–169.
29 A. I. Mazur, E. J. Marcsisin, B. Bird, M. Miljkoviš and M. Diem, *Anal. Chem.*, 2012, **84**, 1259–1266.
30 A. I. Mazur, E. J. Marcsisin, B. Bird, M. Miljković and M. Diem, *Anal. Chem.*, 2012, **84**, 8265–8271.
31 A. Benard, PhD dissertation, Université Libre de Bruxelles, 2012.
32 O. L. Caballero, Q. Zhao, D. Rimoldi, B. J. Stevenson, S. Svobodová, S. Devalle, U. F. Röhrig, A. Pagotto, O. Michielin, D. Speiser, J. D. Wolchok, C. Liu, T. Pejovic, K. Odunsi, F. Brasseur, B. J. Van den Eynde, L. J. Old, X. Lu, J. Cebon, R. L. Strausberg and A. J. Simpson, *PLoS One*, 2010, **5**, 1–7.
33 E. Goormaghtigh and J. Ruysschaert, *Spectrochim. Acta, Part A*, 1994, **50**, 2137–2144.
34 E. Goormaghtigh, *Adv. Biomed. Spectrosc.*, 2009, **2**, 104–128.
35 P. Bassan, A. Kohler, H. Martens, J. Lee, E. Jackson, N. Lockyer, P. Dumas, M. Brown, N. Clarke and P. Gardner, *J. Biophotonics*, 2010, **3**, 609–620.
36 P. Bassan, A. Sachdeva, A. Kohler, C. Hughes, A. Henderson, J. Boyle, J. H. Shanks, M. Brown, N. W. Clarke and P. Gardner, *Analyst*, 2012, **137**, 1370–1377.
37 B. Bird, M. Miljković and M. Diem, *J. Biophotonics*, 2010, **3**, 597–608.
38 R. A. Johnson and D. W. Wichern, in *Applied Multivariate Statistical Analysis*, Prentice Hall, Upper Saddle River, 4th edn, 1998, pp. 726–799.
39 J. H. J. Ward, *J. Am. Stat. Assoc.*, 1963, **58**, 236–244.
40 G. Socrates, in *Infrared and Raman Characteristic Group Frequencies: Tables and Charts*, West Sussex, 3rd edn, 2007.
41 S. J. Gadaleta, E. P. Paschalis, F. Betts, R. Mendelsohn and a. L. Boskey, *Calcif. Tissue Int.*, 1996, **58**, 9–16.
42 E. Goormaghtigh, J.-M. Ruysschaert and V. Raussens, *Biophys. J.*, 2006, **90**, 2946–2957.
43 J. T. Mason and T. J. O'Leary, *J. Histochem. Cytochem.*, 1991, **39**, 225–229.
44 D. C. Fernandez, R. Bhargava, S. M. Hewitt and I. W. Levin, *Nat. Biotechnol.*, 2005, **23**, 469–474.
45 S. I. Nikolaev, D. Rimoldi, C. Iseli, A. Valsesia, D. Robyr, C. Gehrig, K. Harshman, M. Guipponi, O. Bukach, V. Zoete, O. Michielin, K. Muehlethaler, D. Speiser, J. S. Beckmann, I. Xenarios, T. D. Halazonetis, C. V. Jongeneel, B. J. Stevenson and S. E. Antonarakis, *Nat. Genet.*, 2012, **44**, 133–139.
46 F. Draux, C. Gobinet, J. Sulé-Suso, A. Trussardi, M. Manfait, P. Jeannesson and G. D. Sockalingum, *Anal. Bioanal. Chem.*, 2010, **397**, 2727–2737.

47 J.-Y. Chung, T. Braunschweig, R. Williams, N. Guerrero, K. M. Hoffmann, M. Kwon, Y. K. Song, S. K. Libutti and S. M. Hewitt, *J. Histochem. Cytochem.*, 2008, **56**, 1033–1042.
48 M. G. Shim and B. C. Wilson, *Photochem. Photobiol.*, 1996, **63**, 662–671.
49 E. Goormaghtigh, R. Gasper, A. Bénard, A. Goldsztein and V. Raussens, *Biochim. Biophys. Acta, Proteins Proteomics*, 2009, **1794**, 1332–1343.
50 J. W. Chan, D. S. Taylor and D. L. Thompson, *Biopolymers*, 2009, **91**, 132–139.